Two-gap feature in optimally electron-doped cuprates

Wei Hu,[1,2] Zhongpei Feng,[1,2] Jie Yuan,[1] Tao Xiang,[1,2] Dingping Li,[3,*] Baruch Rosenstein,[4,†] Beiyi Zhu,[1] and Kui Jin[1,2]
[1]*Beijing National Laboratory for Condensed Matter Physics, Institute of Physics, Chinese Academy of Sciences, Beijing 100190, China*
[2]*School of Physical Sciences, University of Chinese Academy of Sciences, Beijing 100049, China*
[3]*School of Physics, Peking University, Beijing 100871, China*
[4]*Electrophysics Department, National Chiao Tung University, 30010 Hsinchu, Taiwan, Republic of China*

(Received 27 February 2018; revised manuscript received 6 September 2019; published 19 September 2019)

The dependence of the Hall conductivity on temperature and magnetic field in optimally doped $La_{2-x}Ce_xCuO_{4\pm\delta}$ ($x = 0.105$) thin films demonstrates that both the hole and the electron bands undergo Cooper pairing. The magnetic field suppresses the dominant hole band pairing more effectively, making the subdominant electron band pairing visible. Positively charged Cooper pairs dominate the Hall signal in the mixed state at a weak magnetic field near T_c, while at large field the negatively charged Cooper pairs take over. Sign reversals of the Hall conductivity induced by superconducting fluctuation occur in the transition and can be explained by a weakly coupled two-band Ginzburg-Landau-Lawrence-Doniach model.

DOI: 10.1103/PhysRevB.100.094524

I. INTRODUCTION

Generally, Cooper pairing in complex compounds appears in multiple "pockets" of the Fermi surface, each one characterized by the charge (quasiparticle or hole) and the pairing symmetry (s, d). Indications of the coexistence of an electron and a hole pocket in the normal state of electron-doped cuprates frequently appear in angle-resolved photoemission spectroscopy (ARPES) and magnetotransport. ARPES [1] demonstrated an electron pocket at $(\pi, 0)$ at optimally doped $Nd_{1.85}Ce_{0.15}CuO_{4+\delta}$ (NCCO) to coexist with a new hole pocket at $(\pi/2, \pi/2)$. High-field (up to 60 T) magnetoresistance quantum oscillations in NCCO [2] have also indicated that the two pockets are present near the optimal doping. As for $La_{2-x}Ce_xCuO_4$ and $Pr_{2-x}Ce_xCuO_4$, although there are no similar reports of the spectroscopic results due to the lack of high-quality single crystals, the Hall measurements on their films demonstrate the coexistence of both signs of carriers in $La_{1.895}Ce_{0.105}CuO_4$ and $Pr_{1.85}Ce_{0.15}CuO_4$ (PCCO) [3,4]. Moreover, in the paper by Saadaoui *et al.* [5], in $La_{2-x}Ce_xCuO_{4-\delta}$ with $x = 0.105$, muon spin rotation (μSR) has revealed the absence of a magnetic order, while the angle-dependent magnetoresistance has revealed a sign of the magnetic order/fluctuation which will lead to the Fermi-surface reconstruction and result in the formation of the hole and electron pockets [6,7].

As far as the pairing symmetry is concerned, despite a variety of experimental methods used to investigate the superconducting (SC) state (Raman scattering, ARPES, ac transport, and specific heat), their interpretations still depend on theoretical assumptions. The most important point is the strength of the coupling between the electron and the hole bands. For example, Raman scattering in NCCO [8], ARPES [9] in $Pr_{0.89}LaCe_{0.11}CuO_4$, and the tunneling spectroscopy [10] on PCCO indicated a nonmonotonic d-wave gap dependence on the angle between 0 and $\pi/4$. However, recent ARPES [11] on $Sm_{1.85}Ce_{0.15}CuO_4$ (SCCO) has demonstrated that the gap of the hole pocket is compatible with a monotonic d-wave symmetry, raising the possibility that the nonmonotonic d wave may result from a combination of a d-wave hole gap and an s-wave electron gap. The difference between these two interpretations of experiments might be the strength of the coupling between the two bands (electron and hole). In principle, the temperature dependence of normalized electronic specific heat (the appearance of a "shoulder") is a signature of the coupling strength [12,13]. Unfortunately, the previous measurements of the specific heat of electron-doped cuprates only focused on the low-temperature region where the shoulder was not observed [14,15]. The ac transport data [16] (superfluid density) on PCCO cannot determine the angle dependence, but are inconsistent with a pure d wave. A weakly coupled two-gap model has been proposed to explain the sharp upward curvature in the temperature dependence of superfluid density [17]. As a result, the strength of the coupling between them has become a key issue for understanding the physics of electron-doped cuprates. To address it, one has to return to a more quantitative analysis of the experimental data such as the Hall effect in the SC state.

In the framework of the BCS theory [18–20], the sign of the Hall conductivity ($\sigma_{xy} = \frac{\rho_{xy}}{\rho_{xy}^2+\rho_{xx}^2}$) induced by vortex motion (σ_{xy}^s) near T_c or H_{c2} is the same as that of $\frac{\partial N(\mu)}{\partial \mu}|_{\mu=E_F}$ times the sign of the charge carrier. Here, E_F is the Fermi energy and $N(\mu)$ is the density of states. As for cuprate superconductors, it has been demonstrated by the experiments that the sign of σ_{xy}^s is also closely related to the electronic structure of the vortex [21] which influences the vortex charge accumulated in the vortex core, and subsequently influences the vortex dynamic [22]. As a consequence, if the coupling is weak, the competition between the electron and hole bands may result

*Corresponding author: lidp@pku.edu.cn
†Corresponding author: vortexbar@yahoo.com

in many sign reversals of σ_{xy}^s, since their electronic structures are much different. Therefore, it encourages us to carry out a comprehensive study on the sign reversals in electron-doped cuprates [23–28].

In the present paper, we perform precise Hall measurements on optimally doped $La_{2-x}Ce_xCuO_{4\pm\delta}$ ($x = 0.105$) and fit the results by a weakly coupled two-band Ginzburg-Landau model. σ_{xy}^s in the vortex liquid region have been observed to change from positive to negative as the temperature decreases or field increases. By varying the oxygen content of the sample within a certain range through changing the annealing recipe, the sign reversal can still be observed, indicating that such a phenomenon is intrinsic. Both qualitative and quantitative analyses on such a phenomenon point to a weakly coupled two-gap model, where the hole band dominates the Hall signal in the mixed state near T_c at low magnetic fields, while when the field is increased, the electron band gradually takes over. In the absence of coupling, the model is simplified as that of the hole band with a higher T_c at zero field, while the electron band with a larger H_{c2} at zero temperature.

II. EXPERIMENTAL RESULTS

$La_{1.895}Ce_{0.105}CuO_{4\pm\delta}$ (LCCO) thin films were fabricated by dc magnetron sputtering on (100)-oriented $SrTiO_3$ substrates. The thicknesses of the films are grown higher than 100 nm to eliminate the influence of the thickness on the properties of the films [29]. Patterned into the standard six-probe Hall bridge, the Hall measurements were carried out by Quantum Design PPMS-9 equipment.

For the sample with the optimal annealing condition (S1), the temperature dependences of resistivity ρ_{xx}, conductivity σ_{xx} ($\sigma_{xx} = \frac{\rho_{xx}}{\rho_{xy}^2+\rho_{xx}^2}$), and the Hall conductivity divided by field σ_{xy}/B at different fields are shown in Figs. 1(a)–1(c), respectively (additional results are given in Supplemental Material [30] Fig. S1). As shown in Fig. 1(c), σ_{xy}/B in the normal state undergoes sign changes twice. It can obviously be attributed to the competition between the contributions of the electron and hole bands to the transport. More interestingly, in the mixed state, the behavior of σ_{xy}/B also undergoes a transition, as displayed by the phenomenon in Fig. 1(d) that when the field is decreased, σ_{xy}/B near H_{c2} is increasing at temperatures above 16 K, but decreasing at temperatures below 12 K and first decreasing then increasing in the middle range.

Generally, in the mixed state, the Hall conductivity σ_{xy} consists of two contributions, σ_{xy}^n from the quasiparticles inside the core of the vortices and σ_{xy}^s from the vortex motion. Therefore, in order to clearly observe the evolution of σ_{xy}^s, one should first subtract σ_{xy}^n from σ_{xy}. Since σ_{xy}^n in the normal state is the same as σ_{xy}^n in the mixed state, then if we extract the variation rule of σ_{xy}^n in the normal state, σ_{xy}^n in the mixed state can be obtained following this rule. As for our measurement results, although there is no clear theory yet to describe the relation between σ_{xy}^n/B and B, the dependence of σ_{xy}^n/B on B can be approximately viewed as linear on the scale of the σ_{xy}/B value in the mixed state, as shown in Fig. 1(d) in which the data are cut from Fig. 1(c) by fixed temperatures. Therefore, we fit the field-dependent σ_{xy}^n/B by the linear function in the normal state and extrapolate it to the mixed state to obtain the value of σ_{xy}^n/B in there. Then, we can calculate σ_{xy}^s/B according to $\sigma_{xy}^s/B = \sigma_{xy}/B - \sigma_{xy}^n/B$, where σ_{xy}/B is measured experimentally. As a consequence, field-dependent σ_{xy}^s/B at different temperatures are obtained, as shown in Fig. 2(a). In Figs. 1(d) and 2(a), only several typical temperatures are selected to be displayed. Actually, using the data in Fig. 1(c), we can obtain the field-dependent σ_{xy}/B and subsequently σ_{xy}^s/B at temperatures from 7 to 35 K in intervals of 0.1 K, as shown in Fig. S2 in the Supplemental Material [30]. Then, cutting the data in Fig. S2 by fixed fields, the temperature-dependent σ_{xy}^s/B in Fig. 2(b) can be obtained.

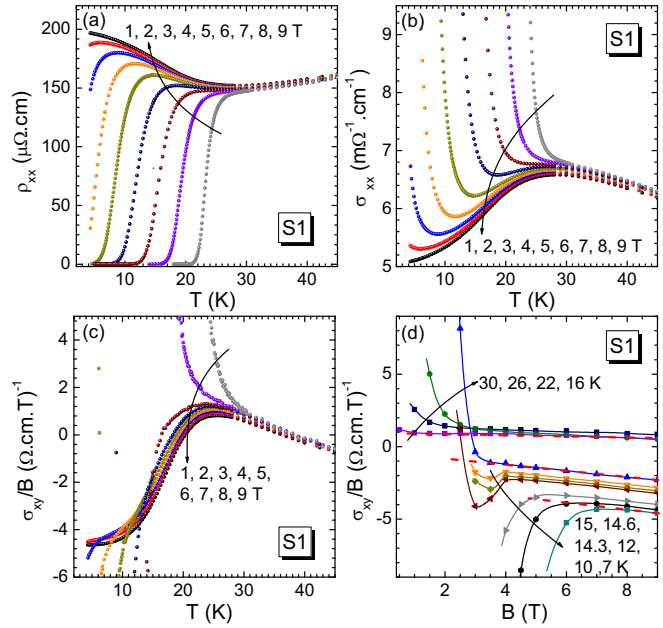

FIG. 1. Temperature dependence of (a) ρ_{xx}, (b) σ_{xx}, and (c) σ_{xy}/B for S1 at constant fields between 1 and 9 T, respectively. (d) Field dependence of σ_{xy}/B at constant temperatures between 7 and 30 K which are extracted from (c). The linear normal parts are highlighted by the red dashed line.

The sign of σ_{xy}^s in Fig. 2(a) separates the temperature range into three parts: positive only from 26 to 16 K, negative only from 12 to 7 K, and an intermediate range where both positive and negative σ_{xy}^s/B appear. Similarly, isomagnetic curves in Fig. 2(b) are also divided into three regions, i.e., positive only from 0.5 to 2.5 T, negative only from 5 to 8 T, and an intermediate range where both positive and negative Hall conductivities appear.

III. REPRODUCIBILITY

For electron-doped cuprates, the measured results of many physical quantities are influenced by sample qualities [31]. So, one may ask whether or not such a previously unrevealed phenomenon is intrinsic. In order to make it clear, first we want to emphasize that this phenomenon happens near T_c or H_{c2} in the mixed state. Previous works, both theoretical [32] and experimental [33] ones, have shown that σ_{xy} will not be influenced by impurities in this region. Second, we have also carried out similar measurements on the other two samples (S2 and S3) with different oxygen contents or annealing

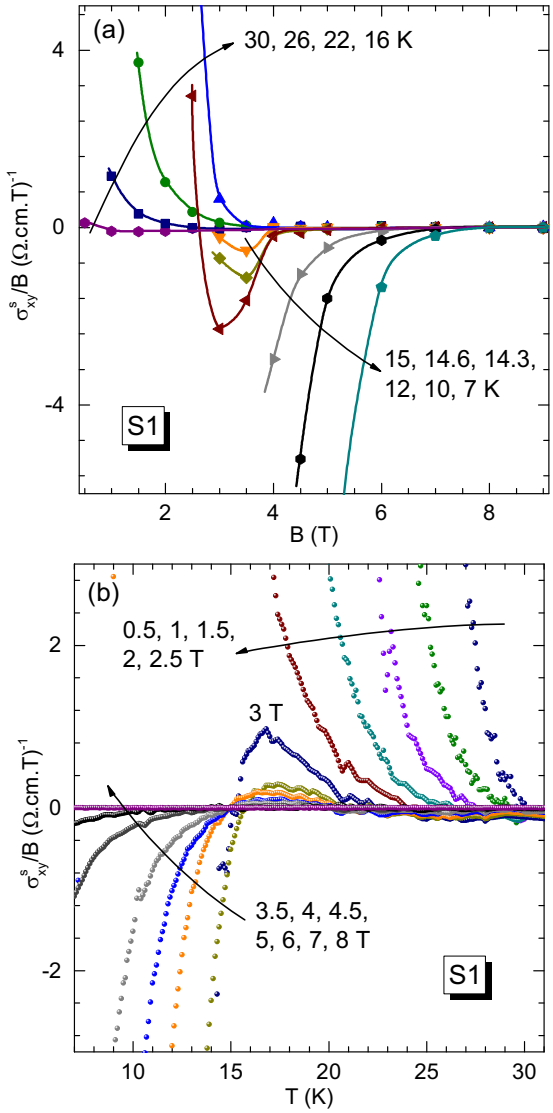

FIG. 2. (a) Field dependence of σ_{xy}^{s}/B at constant temperatures from 10 to 26 K. The solid curves are drawn to guide the eye. (b) Temperature dependence of σ_{xy}^{s}/B at constant fields from 0.5 to 8 T.

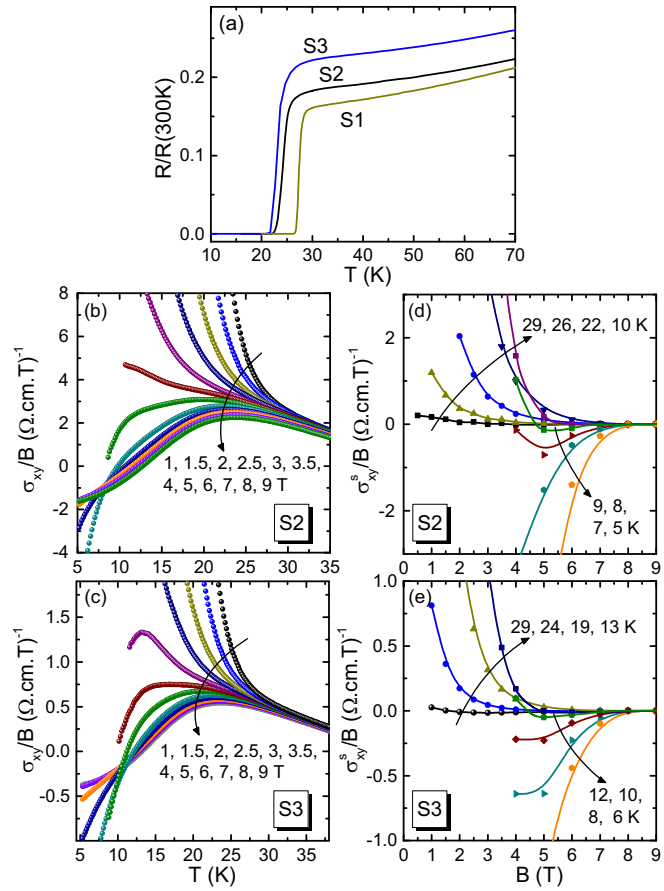

FIG. 3. (a) Temperature dependence of $R/R(300\ \mathrm{K})$ for all the samples. (b) and (c) Temperature dependence of σ_{xy}/B at different fields for S2 and S3, respectively. (d) and (e) Field dependence of σ_{xy}^{s}/B at different temperatures for S2 and S3, respectively.

conditions. Since previous works have shown that the electronic structure can intriguingly vary from two bands to one band for different oxygen contents [34,35], we only tune the oxygen content in a small range here to guarantee the similarity of their electronic structures. As shown in Fig. 3(a), the T_{c0} gradually decreases from S1 to S3, as well as the residual resistivity ratio (RRR). The measured temperature dependence of σ_{xy}/B of S2 and S3 still undergoes the transition described in S1, as displayed by Figs. 3(b) and 3(c). Similarly, we extracted the σ_{xy}^{s}/B of S2 and S3, as shown in Figs. 3(d) and 3(e). The sign of σ_{xy}^{s}/B of both samples still separates the temperature into three parts: positive only at low temperatures, negative only at high temperatures, and alternating in the intermediate range. Consequently, it is reasonable to conclude that such a phenomenon is reproducible within a certain range of oxygen content for LCCO, further providing evidence that it is intrinsic.

IV. QUALITATIVE ANALYSES

As mentioned above, the sign of σ_{xy}^{s} near T_c or H_{c2} is closely related to the electronic structure of the vortex. Given that the electronic structure of the vortex reflects the total fundamental nature of the superfluid electrons and the low-energy excitation of the condensate [22], it can be reasonably deduced that the sign change of σ_{xy}^{s} described in Figs. 2(b) and 2(a) originates from the change of such a fundamental nature. Obviously, such a fundamental nature will not change with varying fields and temperatures for one gap or strongly couple a two-gap scenario, which therefore cannot explain our experimental results.

In the case of the weakly coupled two-gap scenario, a combination of ARPES on SCCO [11] and superfluid density measurements on PCCO [17] indicates that the hole band in optimal electron-doped cuprates dominates the superconducting area near T_c at zero field. Assuming that the positive σ_{xy}^{s} at low fields near T_c shown in Fig. 2(b) comes from the hole band and that the negative σ_{xy}^{s} at high fields comes from the electron band, then the H-T phase diagram should behave as that shown in Fig. 4. This is also consistent with the fact that the Hall conductivity near H_{c2} is positive at high temperatures but negative at low temperatures [Fig. 2(a)]. The gray dashed line represents the transition line of the vortex solid to the

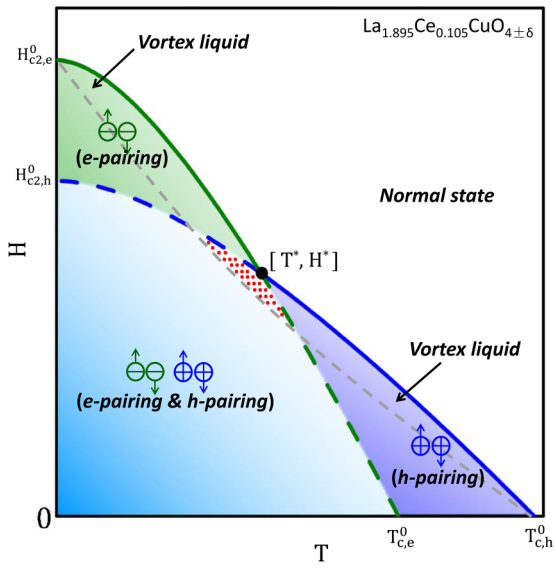

FIG. 4. H-T phase diagram without coupling. The h pairing and e pairing represent the areas dominated by hole and electron Cooper pairs, respectively. $H_{c2,i}$ and $T_{c,i}$ correspond to H_{c2} at zero temperature and T_c at zero field. The subscript $i = e$ or h refers to the electron and hole bands. The blue and the green lines represent the temperature dependence of the upper critical fields for the hole and electron band, respectively, which are stimulated by Werthamer-Helfand-Hohenberg (WHH) theory and their cross point is denoted by $[T^*, H^*]$. The area between the solid curve and the gray dashed line is the vortex liquid region. The area scattered with red dots corresponds to the specific vortex liquid region where hole and electron Cooper pairs compete with each other.

vortex liquid. Inside the vortex liquid phase, in the area scattered with red dots, both the hole and electron Cooper pairs contribute significantly to σ_{xy}^s. Then, the sign reversals in the intermediate field and temperature range in Figs. 2(a) and 2(b) can be naturally attributed to the competition between them.

V. THEORETICAL FITTINGS

Having established the two-band H-T phase diagram based on the qualitative analysis of the experimental results, the transport coefficients are quantitatively analyzed in the framework of the phenomenological Ginzburg-Landau (GL) approach.

The GL approach is the most effective in cases when a microscopic theory is either too complicated or controversial [36]. This is clearly the case in cuprates. However, it still allows us to consider several pairing channels. A well-known example is $YBa_2Cu_3O_{7-\delta}$ (YBCO) in which the dominant d-wave channel is accompanied by the s-wave one [37]. The mean-field GL free energy for a layered material (the Lawrence-Doniach model) with two channels (electron and hole, $i = e, h$) is

$$F_{\rm GL} = d' \sum_{n,i} \int_{\mathbf{r}} \left\{ \frac{\hbar^2}{2m_i} \left|\mathbf{D}\Psi_n^i\right|^2 + \frac{\hbar^2}{2m_c^i d'^2} \left|\Psi_n^i - \Psi_{n+1}^i\right|^2 + \alpha_i \left(T - T_c^{\Lambda,i}\right) \left|\Psi_n^i\right|^2 + \frac{b_i'}{2} \left|\Psi_n^i\right|^4 \right\}. \quad (1)$$

TABLE I. Optimized fitting parameters of S1 in [0.5 T, 2.5 T] and [4.5 T, 8 T] field ranges.

Field range	T_{c0} (K)	H_{c2}^* (T)	γ_n'	κ	γ	η	Λ	d' (Å)
[0.5 T, 2.5 T]	26.5	10.9	0.18	7.38	29	0.0020	0.3	6.225
[4.5 T, 8 T]	18.5	14.3	0.32	3.37	20	−0.0038	0.3	6.225

Here, d' is the distance between layers labeled by n, T_c^{Λ} is the mean-field critical temperature, and m_i and m_c^i are the effective Cooper pair masses in the ab plane ($\mathbf{r}$ position on the plane) and along the c axis, respectively. The covariant derivative, $\mathbf{D} = \nabla - i(e_i^*/\hbar c)\mathbf{A}$, describes the system under constant and homogeneous magnetic field. The homogeneity of the field in the vortex liquid state is ensured for the whole range on magnetic fields considered since Abrikosov vortices strongly overlap [36]. Note that the charge is opposite for particle and hole components, $e_h^* = 2|e| = -e_e^*$. The coupling between channels is neglected (altogether, although its influences have been studied theoretically [37]).

To describe the transport properties at finite temperature, the time-dependent GL equation,

$$\frac{\hbar^2(\gamma' + i\gamma'')}{2m_i} D_\tau \Psi_n^i = -\frac{1}{d} \frac{\delta F_{\rm GL}}{\delta \Psi_n^{*i}} + \zeta_n^i, \quad (2)$$

is used. Here, $D_\tau = \partial_\tau - i(e_i^*/\hbar)\Phi$ is the covariant time derivative, $\gamma' + i\gamma''$ is the complex inverse diffusion constant, of which the tiny imaginary part can be neglected for σ_{xx}, but should be taken into consideration for σ_{xy}, and ζ_n is thermal noise,

$$\langle \zeta_n^*(\mathbf{r}, \tau) \zeta_m(\mathbf{r}', \tau') \rangle = \frac{\hbar^2 \gamma'}{m_i d} T \delta(\mathbf{r} - \mathbf{r}') \delta(\tau - \tau') \delta_{nm}. \quad (3)$$

The nonlinearity of the model is treated by the Gaussian approximation [36] and the expressions of σ_{xx}^s and σ_{xy}^s are derived in the Supplemental Material [30].

Here, we choose the data of S1 to carry in the theoretical analysis. Since the field dependence of σ_{xx}^n is also linear (see Fig. S3 of Supplemental Material [30]), the superconducting contribution σ_{xx}^s is extracted in the same way as σ_{xy}^s. As shown in Fig. 5, the measured temperature dependence of σ_{xx}^s *and* σ_{xy}^s/B from 1 to 2.5 T and 4.5 to 8 T (points) are generally fitted well (lines) by the expression of σ_{xx}^s and σ_{xy}^s derived in the Supplemental Material [30] and the values of parameters listed in Table I. κ is the GL parameter, γ is the anisotropy parameter, Λ is the cutoff energy (in units of $\frac{2e\hbar H_{c2}^*}{mc}$), and H_{c2}^* and η represent $-T_c \frac{dH_{c2}(T)}{dT}|_{T=T_c}$ and $\frac{\gamma''}{\gamma'}$ respectively. γ_n' is the proportionality coefficient between the relaxation time of high T_c superconductors and BCS superconductors, i.e., $\gamma_n' = \frac{\gamma_{\rm BCS}'}{\gamma'}$ and $\gamma_{\rm BCS}' = \frac{\pi\hbar}{8T_c\xi^2}$. Deviations appear at high values of the conductivities. In this region the vortex pinning on the mesoscopic scale should be taken into account. This leads to an underestimated theoretical value in the present calculations. As shown in Table I, the fits to the experimental data in the low- and high-field region lead to two different groups of values, consistent with the H-T phase diagram (Fig. 4). Conductivities at low fields near T_c are dominated by the hole

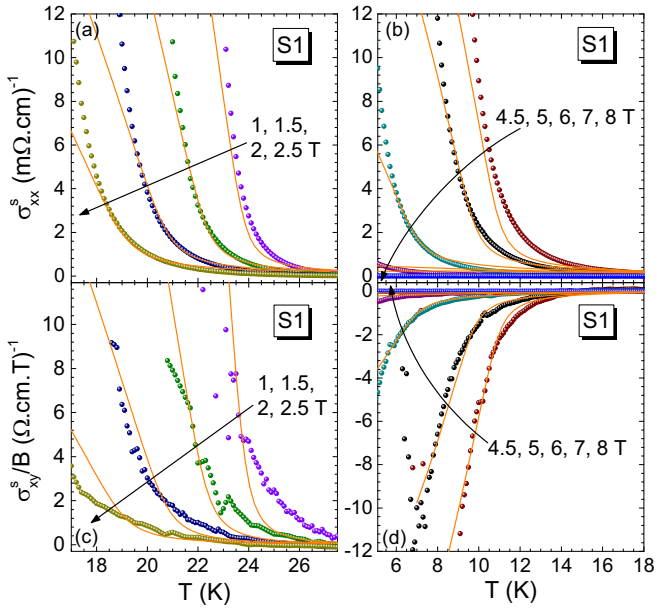

FIG. 5. (a) Temperature dependence of σ^s_{xx} at low magnetic fields between 1 and 2.5 T and high temperatures 18–28 K for S1. The solid curves are the fitting results. Dominated by the hole band. (b) Same for large fields 4.5–8 T and low temperatures 6–18 K. Dominated by the electron band. (c) Temperature dependence of σ^s_{xy}/B at low magnetic fields between 1 and 2.5 T and high temperatures 18–28 K. (d) Same for large fields 4.5–8 T and low temperatures 6–18 K.

band, while at large fields near T_c by the electron band. The sign of η is responsible for the sign reversals of σ^s_{xy}.

VI. CONCLUSIONS AND DISCUSSIONS

In conclusion, the transport properties of the mixed state in optimally doped LCCO under a magnetic field to probe the multicomponent character of the superconducting gap were studied experimentally and theoretically. The magnetoresistance and Hall data are explained both qualitatively and quantitatively in terms of a weakly coupled two-band model in the vortex liquid region of the magnetic phase diagram, providing important information to clarify the pairing symmetry of the electron-doped cuprates. The hole band Cooper pairing dominates the signal in the mixed state near T_c at low fields, while the electron band gradually takes over when the field is increased. The magnetic field therefore suppresses the majority hole band pairing more effectively than the minority electron band pairing. A similar structure of the magnetic phase diagram can also been established in $Sm_{1.85}Ce_{0.15}CuO_4$ [28] and PCCO [26], indicating that it is a general property for optimal electron-doped cuprates.

The analysis of the transport data was based solely on the phenomenological two-band Ginzburg-Landau-Lawrence-Doniach approach rather than a microscopic one, so that it is applicable to similar cases as well. In many other layered compounds, several pairing channels are present, although in most cases the charge of the Cooper pair is the same. Experimentally, it is difficult to demonstrate the multiband nature via vortex physics, since the contributions to the Hall conductivity do not "compete" (the best studied example being the hole-doped cuprate YBCO [37]). In such cases, the coupling between the pairing channels is not negligible. The theory can in principle be extended to a stronger coupling between the two pairing channels.

ACKNOWLEDGMENTS

We acknowledge Jérémy Brisbois and Yu Wang for their help. This work was supported by the National Key Basic Research Program of China (2015CB921000 and 2016YFA0300301), the National Natural Science Foundation of China (11674374, 11474338, and 11674407), the Key Research Program of Frontier Sciences, CAS (QYZDB-SSW-SLH008), and the Strategic Priority Research Program of the CAS (XDB07020100 and XDB07030200), the Beijing Municipal Science and Technology Project (Z161100002116011).

[1] N. P. Armitage, F. Ronning, D. H. Lu, C. Kim, A. Damascelli, K. M. Shen, D. L. Feng, H. Eisaki, Z.-X. Shen, P. K. Mang, N. Kaneko, M. Greven, Y. Onose, Y. Taguchi, and Y. Tokura, Phys. Rev. Lett. **88**, 257001 (2002).

[2] T. Helm, M. V. Kartsovnik, M. Bartkowiak, N. Bittner, M. Lambacher, A. Erb, J. Wosnitza, and R. Gross, Phys. Rev. Lett. **103**, 157002 (2009).

[3] K. Jin, B. Y. Zhu, B. X. Wu, L. J. Gao, and B. R. Zhao, Phys. Rev. B **78**, 174521 (2008).

[4] Y. Dagan, M. M. Qazilbash, C. P. Hill, V. N. Kulkarni, and R. L. Greene, Phys. Rev. Lett. **92**, 167001 (2004).

[5] H. Saadaoui, Z. Salman, H. Luetkens, T. Prokscha, A. Suter, W. A. MacFarlane, Y. Jiang, K. Jin, R. L. Greene, E. Morenzoni, and R. F. Kiefl, Nat. Commun. **6**, 6041 (2015).

[6] J. Lin and A. J. Millis, Phys. Rev. B **72**, 214506 (2005).

[7] C. Kusko, R. S. Markiewicz, M. Lindroos, and A. Bansil, Phys. Rev. B **66**, 140513(R) (2002).

[8] G. Blumberg, A. Koitzsch, A. Gozar, B. S. Dennis, C. A. Kendziora, P. Fournier, and R. L. Greene, Phys. Rev. Lett. **88**, 107002 (2002).

[9] H. Matsui, K. Terashima, T. Sato, T. Takahashi, M. Fujita, and K. Yamada, Phys. Rev. Lett. **95**, 017003 (2005).

[10] Y. Dagan, R. Beck, and R. L. Greene, Phys. Rev. Lett. **99**, 147004 (2007).

[11] A. F. Santander-Syro, M. Ikeda, T. Yoshida, A. Fujimori, K. Ishizaka, M. Okawa, S. Shin, R. L. Greene, and N. Bontemps, Phys. Rev. Lett. **106**, 197002 (2011).

[12] M. Zehetmayer, Supercond. Sci. Technol. **26**, 043001 (2013).

[13] E. J. Nicol and J. P. Carbotte, Phys. Rev. B **71**, 054501 (2005).

[14] W. Yu, B. Liang, and R. L. Greene, Phys. Rev. B **72**, 212512 (2005).

[15] G. M. Zhao and J. Wang, J. Phys.: Condens. Matter **22**, 352202 (2010).

[16] M.-S. Kim, J. A. Skinta, T. R. Lemberger, A. Tsukada, and M. Naito, Phys. Rev. Lett. **91**, 087001 (2003).
[17] H. G. Luo and T. Xiang, Phys. Rev. Lett. **94**, 027001 (2005).
[18] H. Fukuyama, H. Ebisawa, and T. Tsuzuki, Prog. Theor. Phys. **46**, 1028 (1971).
[19] N. B. Kopnin, B. I. Ivlev, and V. A. Kalatsky, J. Low Temp. Phys. **90**, 1 (1993).
[20] R. J. Troy and A. T. Dorsey, Phys. Rev. B **47**, 2715 (1993).
[21] T. Nagaoka, Y. Matsuda, H. Obara, A. Sawa, T. Terashima, I. Chong, M. Takano, and M. Suzuki, Phys. Rev. Lett. **80**, 3594 (1998).
[22] K.-i. Kumagai, K. Nozaki, and Y. Matsuda, Phys. Rev. B **63**, 144502 (2001).
[23] P. Seng, J. Diehl, S. Klimm, S. Horn, R. Tidecks, K. Samwer, H. Hänsel, and R. Gross, Phys. Rev. B **52**, 3071 (1995).
[24] T. B. Charikova, N. G. Shelushinina, G. I. Harus, D. S. Petukhov, A. V. Korolev, V. N. Neverov, and A. A. Ivanov, Physica C: Superconductivity **483**, 113 (2012).
[25] K. Jin, B. X. Wu, B. Y. Zhu, B. R. Zhao, A. Volodin, J. Vanacken, A. V. Silhanek, and V. V. Moshchalkov, Physica C: Superconductivity **479**, 53 (2012).
[26] K. Jin, W. Hu, B. Zhu, D. Kim, J. Yuan, Y. Sun, T. Xiang, M. S. Fuhrer, I. Takeuchi, and R. L. Greene, Sci. Rep. **6**, 26642 (2016).
[27] S. J. Hagen, A. W. Smith, M. Rajeswari, J. L. Peng, Z. Y. Li, R. L. Greene, S. N. Mao, X. X. Xi, S. Bhattacharya, Q. Li, and C. J. Lobb, Phys. Rev. B **47**, 1064 (1993).
[28] M. Cagigal, J. Fontcuberta, M. A. Crusellas, J. L. Vicent, and S. Pinol, Physica C: Superconductivity **248**, 155 (1995).
[29] B. X. Wu, K. Jin, J. Yuan, H. B. Wang, T. Hatano, B. R. Zhao, and B. Y. Zhu, Supercond. Sci. Technol. **22**, 085004 (2009).
[30] See Supplemental Material at http://link.aps.org/supplemental/10.1103/PhysRevB.100.094524 for additional experimental results and detailed derivation processes of the σ^s_{xx} and σ^s_{xy} expressions.
[31] N. P. Armitage, P. Fournier, and R. L. Greene, Rev. Mod. Phys. **82**, 2421 (2010).
[32] V. M. Vinokur, V. B. Geshkenbein, M. V. Feigelman, and G. Blatter, Phys. Rev. Lett. **71**, 1242 (1993).
[33] A. V. Samoilov, A. Legris, F. Rullier-Albenque, P. Lejay, S. Bouffard, Z. G. Ivanov, and L.-G. Johansson, Phys. Rev. Lett. **74**, 2351 (1995).
[34] M. Horio, T. Adachi, Y. Mori, A. Takahashi, T. Yoshida, H. Suzuki, L. C. C. Ambolode, K. Okazaki, K. Ono, H. Kumigashira, H. Anzai, M. Arita, H. Namatame, M. Taniguchi, D. Ootsuki, K. Sawada, M. Takahashi, T. Mizokawa, Y. Koike, and A. Fujimori, Nat. Commun. **7**, 10567 (2016).
[35] M. Horio, Y. Krockenberger, K. Koshiishi, S. Nakata, K. Hagiwara, M. Kobayashi, K. Horiba, H. Kumigashira, H. Irie, H. Yamamoto, and A. Fujimori, Phys. Rev. B **98**, 020505(R) (2018).
[36] B. Rosenstein and D. Li, Rev. Mod. Phys. **82**, 109 (2010).
[37] M. Yethiraj, H. A. Mook, G. D. Wignall, R. Cubitt, E. M. Forgan, D. M. Paul, and T. Armstrong, Phys. Rev. Lett. **70**, 857 (1993); B. Keimer, W. Y. Shih, R. W. Erwin, J. W. Lynn, F. Dogan, and I. A. Aksay, *ibid.* **73**, 3459 (1994); Y. Ren, J. H. Xu, and C. S. Ting, *ibid.* **74**, 3680 (1995); C. Y. Mou, R. Wortis, A. T. Dorsey, and D. A. Huse, Phys. Rev. B **51**, 6575 (1995); M. Franz, C. Kallin, P. I. Soininen, A. J. Berlinsky, and A. L. Fetter, *ibid.* **53**, 5795 (1996).